CONF-8510168--3

EFFECT OF MICROSTRUCTURE ON THE ARSENIC PROFILE IN IMPLANTED SILICON

W. A. Coghlan
M. H. Rhee
Mechanical and Aerospace Engineering
Arizona State University
Tempe, Arizona 85287

J. M. Williams
Solid State Physics Division
Oak Ridge National Laboratory
Oak Ridge, Tennessee 37830

CONF-8510168--3

DE86 003272

L. A. Streit
P. Williams
Center for Solid State Science
Arizona State University
Tempe, Arizona 85287

ABSTRACT

According to an irradiation damage model, the profile of an implanted ion at temperature great enough for diffusion to occur will depend on the sink density in the material. To test this model, pure silicon wafers were prepared with high and low dislocation densities. These wafers were implanted with about 5×10^{17} As^{+2}/m^2 at 77°K, 300°C, and 600°C. After implanting the profiles were measured using Rutherford backscattering spectroscopy and secondary ion mass spectroscopy. The observed spreading of the As-profile contradicts initial theoretical predictions. Further speculation is presented to explain the differences.

MASTER

1. Introduction

Ion implantation is becoming a common method for improving the surface properties of many materials, but in the semiconductor industry it has become a major production process. Most semiconductor devices have been ion implanted and many of them have

DISCLAIMER OF THIS DOCUMENT IS CRU...

been implanted several times with various ions and energies [1]. In general the irradiation damage that is introduced during implantation at ambient temperature is removed by a following high temperature anneal. This process is not entirely satisfactory since some electrically active defects still remain after annealing [2,3], and in some cases residual damage is desirable as in the case of using ion implantation damage as sites for gettering impurities [4]. In order to improve these processes and to minimize the detrimental effects, it is necessary to understand the irradiation damage.

The distribution of implanted ions and the damage energy in layered semiconductor materials have been calculated using the Boltzmann equation [5]. Manning and Mueller [6] developed a computer program called EDEP-1 for performing similar calculations for irradiation damage research. In both of these calculations and the modifications that follow the processes considered are those immediately after the ion implant. No thermally activated processes such as diffusion have been considered. As a result these calculations have been the starting point for the development of radiation damage theory. At temperatures where diffusion can occur the implanted ions and the lattice damage are treated using chemical rate theory and the development of defect clusters, dislocation loops, bubbles, and voids can be considered as radiation continues. Yoo and Mansur [7,8] have specifically considered the development of damage in the surface region of a sample under ion bombardment. In these calculations the conditions were specifically chosen to simulate radiation damage in structural

materials for nuclear applications.

The radiation damage model was modified to include the diamond cubic or zinc blende crystal structure of semiconductor materials. In irradiation damage in structural alloys most of the defects produced diffuse to sinks such as cavities or dislocations. In semiconductors the sink strengths will be several orders of magnitude lower than in metals since the dislocation density is much lower. Several calculations were made using much lower sink strengths with the idea that most defects will annihilate defects of the opposite kind. In this situation the average lifetime of the defects is much longer and so the average concentration is much higher and the defects diffuse over much greater distances.

The model was also modified to account for the profile of the implanted ions. It was found that at temperatures where diffusion occurs the final profile of the implanted ions broadened considerably and depended on the sink strength. In Fig. 1 the concentration of implanted ions is shown as a function of depth for two different sink strengths. It is immediately obvious that there is a "tail" extending deep in the crystal and that this "tail" is much more pronounced for low dislocation density than for high dislocation density. The reason is that the lifetime of the defects is much longer for low dislocation density. We then designed this experiment to validate the irradiation damage model approach to this problem.

Sample of undoped Czochralski silicon were obtained with high and low dislocation density. Arsenic ions were implanted at 300°C and 600°C and careful measurement of the resulting arsenic

atom profiles were made using Rutherford backscattering spectroscopy (RBS) and secondary ion mass spectroscopy (SIMS). An additional implantation was performed at 77°K on the assumption that no broadening would occur at this temperature. At this temperature the arsenic is expected to remain where it is implanted. Each of these experimental steps is described below.

2. Preparation of Silicon Samples

A special undoped 7 kg Czochralski silicon crystal was growth at the crystal growing facilities of Monsanto Corporation. As the crystal reached the final desired length, it was suddenly pulled from the melt. This event sometimes occurs during the growth of commercial crystals and results in severe damage of the crystal. As a result of the sudden change in hydrodynamic forces and large thermal stress coupled with the high temperature of the crystal, large numbers of dislocations are formed in a region about two diameters of the crystal in length. Since the crystal was about 92 mm in diameter, a region of about 180 mm was expected to have a much higher dislocation density than the main body of the crystal. In commercial silicon wafers "low dislocation densities" often mean "dislocation free" silicon. In such crystals there are no long network dislocations and only a few dislocation loops.

Wafers were cut and polished at Motorola Semiconductor Products, Inc. from silicon cut from two locations of the crystal as shown in Fig. 2. After polishing the wafers were given a standard chemical polish to remove the layer damaged during the polishing. The wafers from near the center of the crystal are standard "dislocation free" silicon which we designate as "low

dislocation density" in the remainder of this paper. Wafers cut near the damaged end are designated "high dislocation density." The high dislocation silicon was cut from material about 100 mm from the damaged end. Although this position is less desirable than nearer the end, it was done because of difficultly encountered in cutting near the damaged end. The high stresses present in the damaged region lead to sudden fracture of the material as it was being cut.

In spite of the difficulty in cutting the material, etching results have shown that there are differences in the defect density between the two kinds of wafers. Initial etching experiments, using the Sirtl [9] etch, revealed a moderate density of irregular pits from "swirl defects" [10] with a few possible dislocation pits in the high dislocation density material. In order to distinguish between the two types of defects a sample of each material was marked with four microhardness pits. The samples were etched and photographed, were polished and re-etched. All the small irregular pits disappeared and were replaced by a new array. Several pits in the high dislocation density material reappeared in the same position. No pits reappeared in the low dislocation density material. As a result of these measurements an approximate dislocation density of 10^7 m^{-2} was measured in the high dislocation density material. The low dislocation density material was dislocation free. A difference in the density of irregular pits was also seen. After an etch of 95 s, densities of 7.4×10^9 and 1.0×10^9 pits/m^2 were seen in the high and low dislocation density material, respectively. The volume density of these defects is not

known because the thickness of the material removed during etching is not known, however the relative difference in the two materials should be correct since the same amount of material was removed from both materials.

Transmission electron microscopy of the sample ion implanted at 600°C was attempted. The sample was backthinned by mechanical polishing followed by ion milling. Using this process the implanted region can be seen since the depth of the implant is about 0.2 μm. Very few dislocations (one) were seen, but a number of octahedral precipitates (probably oxide precipitates) with a strain contrast field surrounding them. It is not known if these precipitates formed during ion implantation or during the growth. More TEM is planned.

3. Ion Implantation

Samples of each material were implanted at the Surface Modification and Characterization Collaborative Research Center at the Oak Ridge National Laboratory. The silicon wafers were cleaved into 20 mm squares and were mounted on a sample holder designed for elevated temperature implants. The samples were mounted in pairs of high and low dislocation density and implants were conducted at each temperature in turn. Part of the samples were masked so that ion beams channeling experiments could be performed. The temperature was controlled to ±2°C and the vacuum in the sample chamber was at 1 x 10^{-6} torr or better. The irradiation dose was controlled by integrating the ion current to a fixed value giving a nominal concentration of 4.3 x 10^{19} As^{+2}/m^2 at 290 KeV. In

addition to these samples, a sample of low dislocation material was implanted at 77°K.

The 300°C implants were done first with the 600°C following. The temperature was achieved after heating for about 30 minutes the the two implants at each temperature followed each other by about 4 minutes. Since the high dislocation samples were implanted first, each experienced a few minute anneal at the irradiation temperature after they were implanted. One goal of future modeling efforts will be to determine if this anneal is important.

4. Chemical Analysis of Arsenic Profiles

After implanting, the As-profiles were measured using RBS and SIMS. Both techniques were used because they each offer unique properties. The RBS, which was conducted with the ion implantation at Oak Ridge National Laboratory using 2 MeV α^+ ions, gives the concentration profile along with an accurate measure of the total integrated arsenic concentration. SIMS is more sensitive to low concentrations and will thereby extend the range, but it is not easy to obtain absolute concentrations. RBS is a nondistructive technique which can be repeated on the same sample. SIMS requires ion sputtering the surface to measure depth profiles.

Depth profiles of the samples were measured by SIMS using the Cameca IMS-3F ion microprobe. The Cs^+ primary beam (14.5 keV impact energy at 470-490 nA) was rastered over a 250 μm^2 area. The negative secondary ions that were monitored were restricted by a physical aperture to a 62 μm diameter circle within the analyzed

area, thereby, eliminating ions sputtered from the crater walls. Silicon secondary ions were counted by a Faraday cup and arsenic ions by using an electron multiplier. Crater depths were obtained using a Sloan Dektak stylus profilometer. Sputtering time scales were converted to depth scales using the Dektak measurements assuming a constant sputtering rate.

The resulting profiles are shown in Figs. 3-6. In these figures the small circles are the RBS data and the solid lines are SIMS profiles of the same samples which have been normalized to the same maximum value. Several obvious characteristics can be seen. First the shape of the SIMS results is nearly the same as that seen from the RBS. Also there are obvious differences in the profiles; the experiment is successful in that changes in microstructure and temperature affects the implanted profile.

The linear concentration plots shown in Figs. 3-6 are very useful in showing the equivalence of the two methods but increased sensitivity is one of the advantages of SIMS. The same SIMS profiles are shown in Figs. 7 and 8 in a log concentration versus depth. These plots emphasize the difference in the profiles. In addition to these profiles the profile of the sample implanted at 77°K is given in Fig. 9. As expected this profile shows the least broadening.

5. Discussion and Conclusions

Ion implantation at different temperatures and in material containing different defect densities results in different arsenic profiles. The maximum concentration is different and the width of

the profiles are different. The width of the profiles for each case is shown in Table I for both RBS and SIMS along with the integrated arsenic concentration measured by RBS. Several important observations can be made. In all cases the As-profiles are broadened by increasing the implant temperature and also by increasing the defect density. This observation is in opposition to the original calculation which predicted a narrower profile for a higher sink strength. Another interesting result is that the profile is broadened more at 300°C than at 600°C. This result may be expected since defect recombination is expected to increase with increased temperature and the corresponding defect lifetime will decrease.

At 77°K there is also a difference between the measured and the calculated profiles. The EDEP-1 calculations shown in Fig. 10 show an expected arsenic profile with a maximum at 0.16 μm with a standard deviation of 0.05 μm. The values measured by SIMS are 0.19 μm and 0.11 μm respectively. Perhaps some irradiation broadening has occurred at this temperature also.

The fact that the profiles are broadened at 300°C implies that point defect diffusion occurs at this temperature and that the diffusion of arsenic is coupled with the flow of defects. The fact that more broadening was seen at 300°C than at 600°C indicates there is stronger binding between the arsenic at the lower temperature. This would be expected if thermal energy at 600°C is sufficient to reduce the number of arsenic-defect pairs. The effect of defect concentration can be explained if the major effect is a result of quenched in point defects and defect clusters and

not the dislocations and swirl defects. Further modeling will be done to investigate this point. It seems that pipe diffusion along dislocation cores is unlikely because of the low dislocation density.

The original model had very simple irradiation induced segregation which did not include any binding between the arsenic ions and the defects. It included segregation coupled with the vacancy flux. As vacancies diffused away from the damage region arsenic was also moved. There is some evidence [12] that arsenic diffuses with an interstitial mechanism and it is necessary that the model be expanded to include segregation mechanisms which include interstitial diffusion.

Along with the difference in quenched-in defects another difference between the materials may be important. There is an oxygen gradient along the crystal with higher oxygen in the low dislocation material than in the high dislocation material. It is interesting to note that a higher density of swirl defects is observed in the high defect density material. If these defects were related to the presence of oxide precipitates, the opposite would be expected.

Our plans for future work include more TEM characterization of the starting materials and also the structure present after ion implantation. We plan to couple future experiments with electrical measurements to correlate the results with processing variables. The channeling data which were taken will be analyzed to determine the lattice position of the arsenic and also the relative damage condition of the silicon before and after implantation.

In conclusion this investigation has shown that As^{+2} implantation is effected by changing the implant temperature and also by changing the initial defect structure of the silicon. Increasing the temperature increases the width of the implanted arsenic profile especially at 300°C. Increasing the initial defect density appears to also increase the width of the profile.

Acknowledgments

We would like to acknowledge the support of this research by John Holder at Monsanto Corporation who provided the silicon ingot, and to Frank Garcia at Motorola Semiconductor Products, Inc. who cut and polished the wafers. In addition we acknowledge the help of D. D. Perry and Steve Lakomski who performed the computer calculations. The support of NSF Grant DMR 8206028 is acknowledged for the SIMS measurement. The ion implantation and RBS measured at Oak Ridge National Laboratory is provided under DOE Contract No. DE-AC05-840R21400. Finally the support of Arizona State University through Faculty Grant in Aids for 1983 and 1985 is appreciated.

References

[1] Amitabh Jain, Rad. Eff. 63 (1982) 39.
[2] J. Krynicki & J.C. Bourgoin, Nucl. Instrum. Meth. Phys. Res. 209/210 (1983) 437-440.
[3] D. Hagmann, Nucl. Instrum. Meth. Phys. Res. 209/210 (1983) 683-687.
[4] D. Lecrosnier, Nucl. Instrum. Meth. Phys. Res. 209/210 (1983) 325-332.
[5] L. A. Christel, J.F. Gibbons, & S. Mylroie, J. Appl. Phys. 51 (1980) 6176-6182.
[6] Irwin Manning and G.P. Mueller, Computer Phys. Comm. 7 (1974) 85-94.
[7] M.H. Yoo and L.K. Mansur, J. Nucl. Mater. 62 (1976) 282.
[8] M.H. Yoo, J. Nucl. Mater. 68 (1977) 193.
[9] Von Erhard Sirtl and Annemarie Adler, Z. Metallkde 52 (1961) 529-531.
[10] K.V. Ravi, Imperfections and Impurities in Semiconductor Silicon, John Wiley & Sons, 1981, p.66.
[11] E. Nygren, M.J. Aziz, D. Turnbull, J.M. Poate, D.C. Jacobson, and R. Hull, Appl. Phys. Lett. 47 (1985)105.

TABLE I
SUMMARY OF ANALYTICAL MEASUREMENTS

SAMPLE	WIDTH AT HALF-HEIGHT, μm		As^{+2}/m^2
	SIMS	RBS	(x 10^{19})
77°K	0.18	---	---
Low Defect Density			
300°C			
Low Defect Density	0.19	0.23	4.49
High Defect Density	0.36	0.32	3.84
600°C			
Low Defect Density	0.19	0.21	4.11
High Defect Density	0.22	0.23	4.90

Figure Captions

Figure 1: Implanted ion concentration as a function of depth (a) High dislocation density, and (b) Low dislocation density.

Figure 2: Diagram showing how the damaged crystal was cut.

Figure 3: RBS and SIMS concentration profiles for As^{+2} implants on low dislocation density silicon at 300°C. The open circles are RBS data and while the solid line is SIMS.

Figure 4: RBS and SIMS concentration profiles for As^{+2} implants on high dislocation density silicon at 300°C. The open circles are RBS data and while the solid line is SIMS.

Figure 5: RBS and SIMS concentration profiles for As^{+2} implants on low dislocation density silicon at 600°C. The open circles are RBS data and while the solid line is SIMS.

Figure 6: RBS and SIMS concentration profiles for As^{+2} implants on high dislocation density silicon at 600°C. The open circles are RBS data and while the solid line is SIMS.

Figure 7: As^{+2} ion profiles for implants at 300°C measured by SIMS. The narrower profile is for low dislocation density material while the wider profile is for high dislocation density.

Figure 8: As^{+2} ion profiles for implants at 600°C measured by SIMS. The narrower profile is for low dislocation density material while the wider profile is for high dislocation density.

Figure 9: As^{+2} ion profiles for implants at 77°K measured by SIMS.

Figure 10: Calculation of the implanted ion profile and the damage energy for 290 keV As^{+2} ions on silicon.

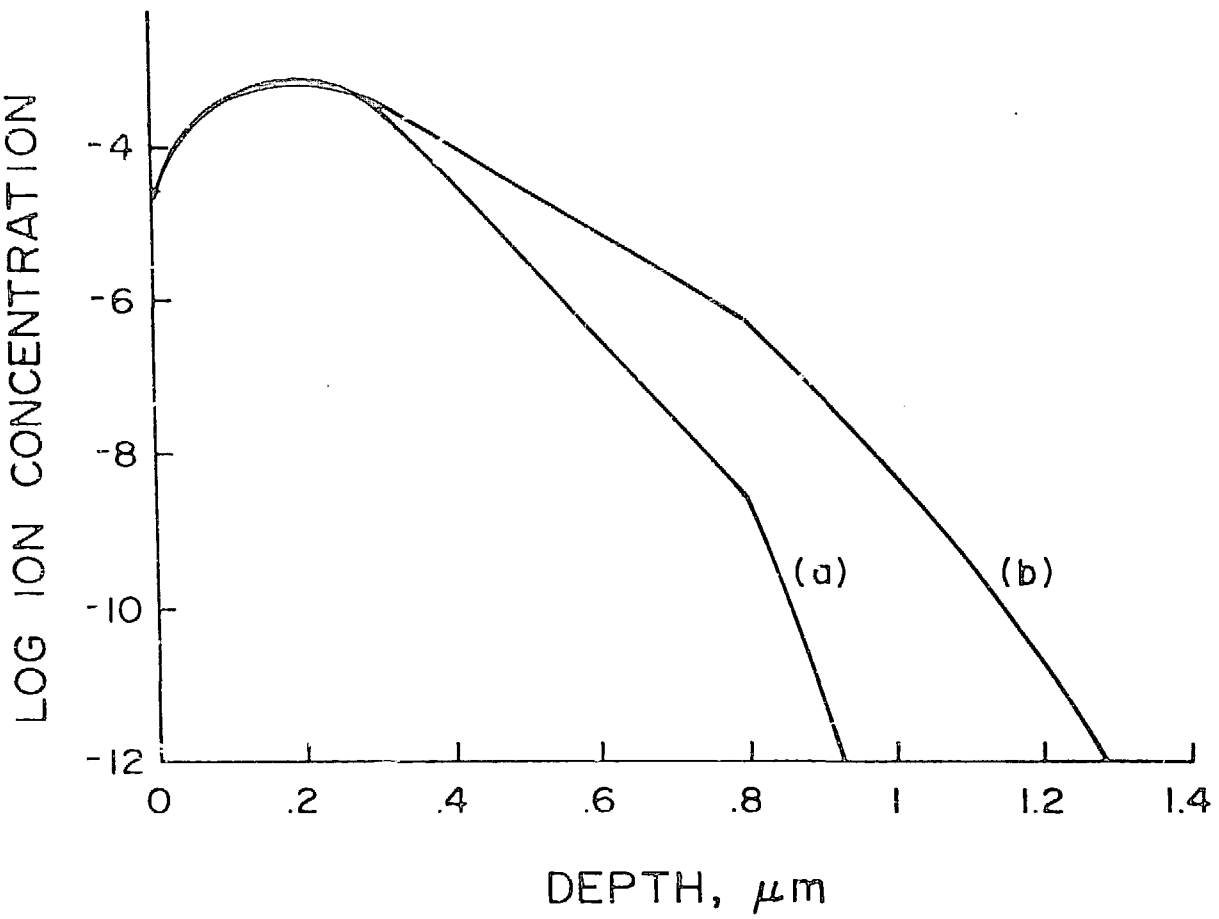
LOG ION CONCENTRATION
-4
-6
-8
-10
-12
0
.2
.4
.6
.8
1
1.2
1.4
(a)
(b)
DEPTH, μm

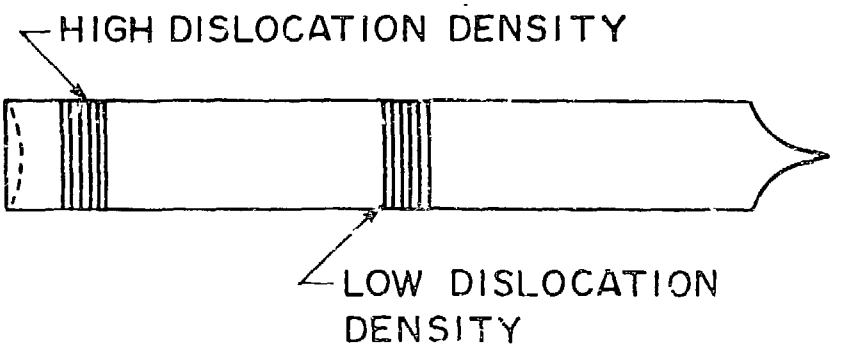

Figure 2

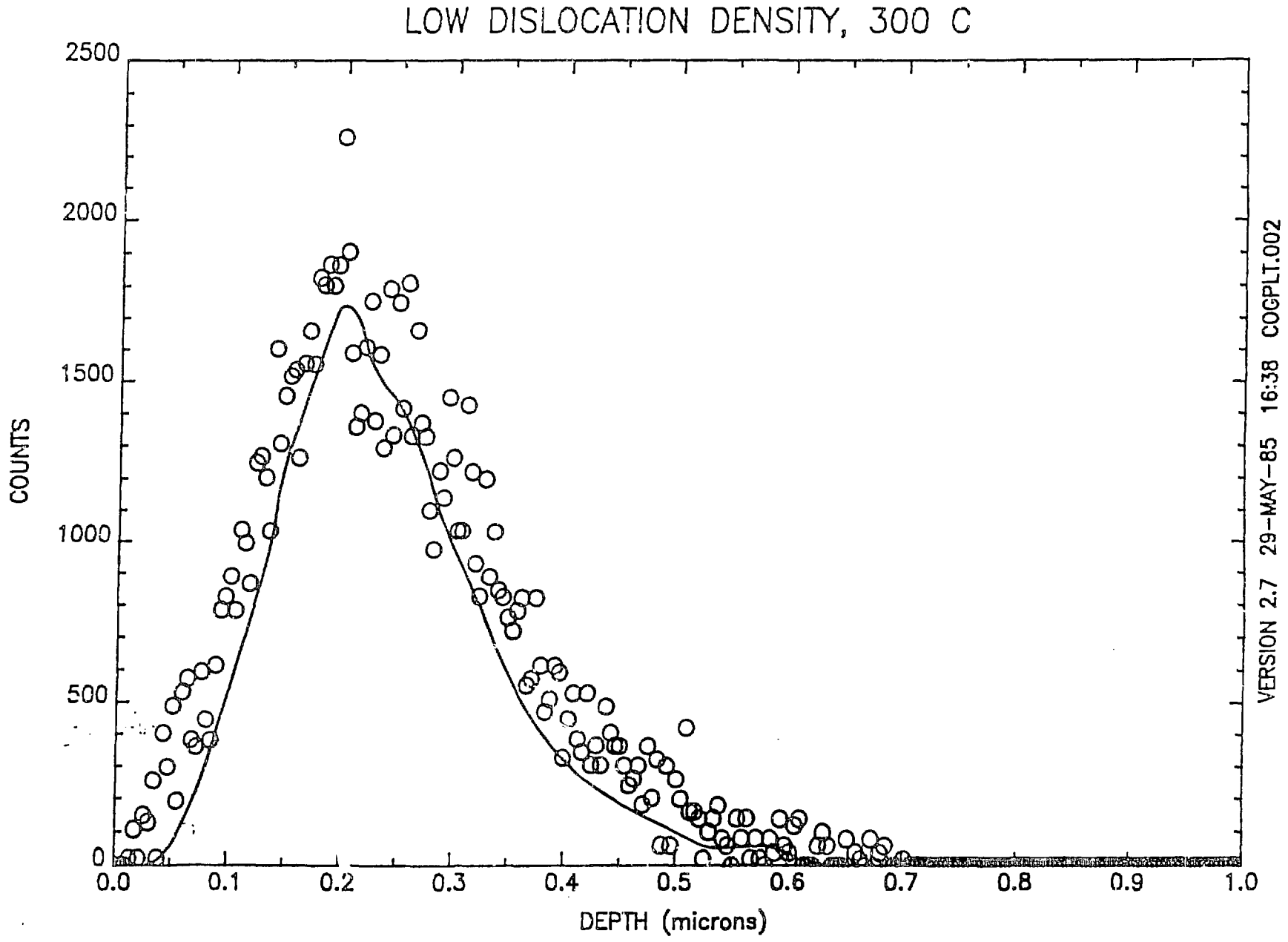
LOW DISLOCATION DENSITY, 300 C
2500
2000
1500
1000
500
0
COUNTS
0.0
0.1
0.2
0.3
0.4
0.5
0.6
0.7
0.8
0.9
1.0
DEPTH (microns)
VERSION 2.7 29-MAY-85 16:38 COGPLT.002

Figure 3

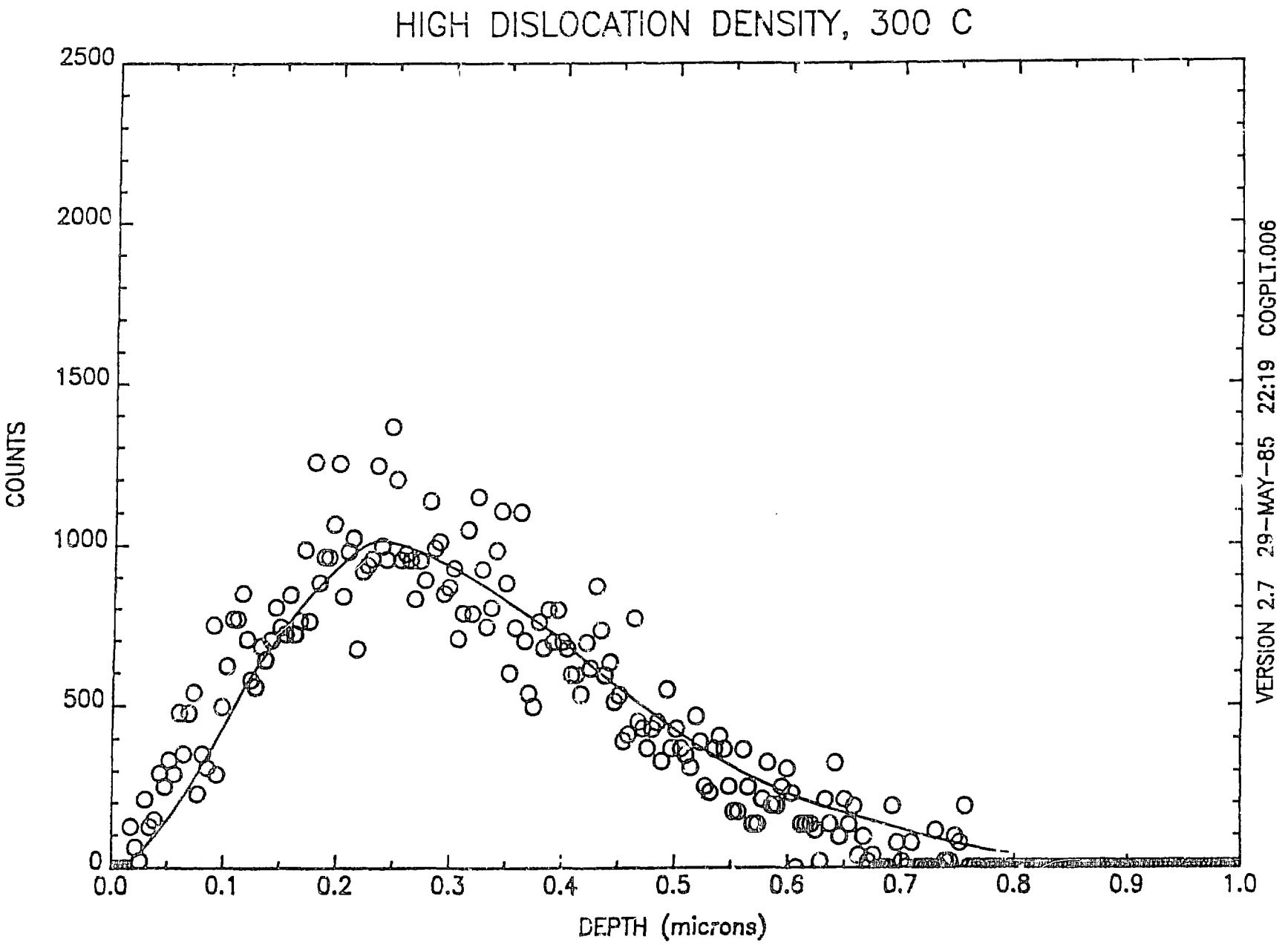
HIGH DISLOCATION DENSITY, 300 C
COUNTS
2500
2000
1500
1000
500
0
0.0
0.1
0.2
0.3
0.4
0.5
0.6
0.7
0.8
0.9
1.0
DEPTH (microns)
VERSION 2.7 29-MAY-85 22:19 COGPLT.006

Figure 4

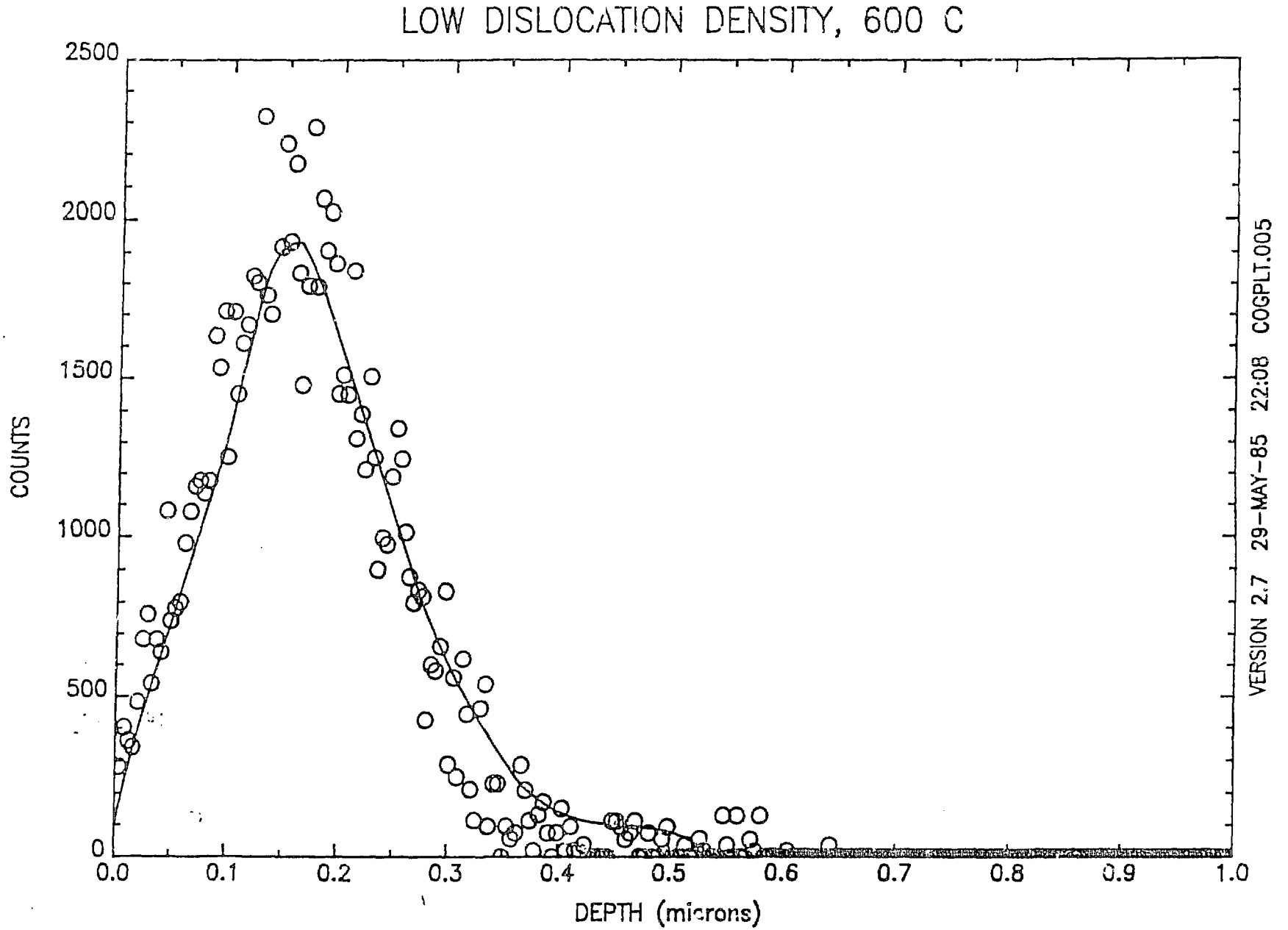
LOW DISLOCATION DENSITY, 600 C
2500
2000
1500
1000
500
0
COUNTS
0.0
0.1
0.2
0.3
0.4
0.5
0.6
0.7
0.8
0.9
1.0
DEPTH (microns)
VERSION 2.7 29-MAY-85 22:08 COGPLT.005

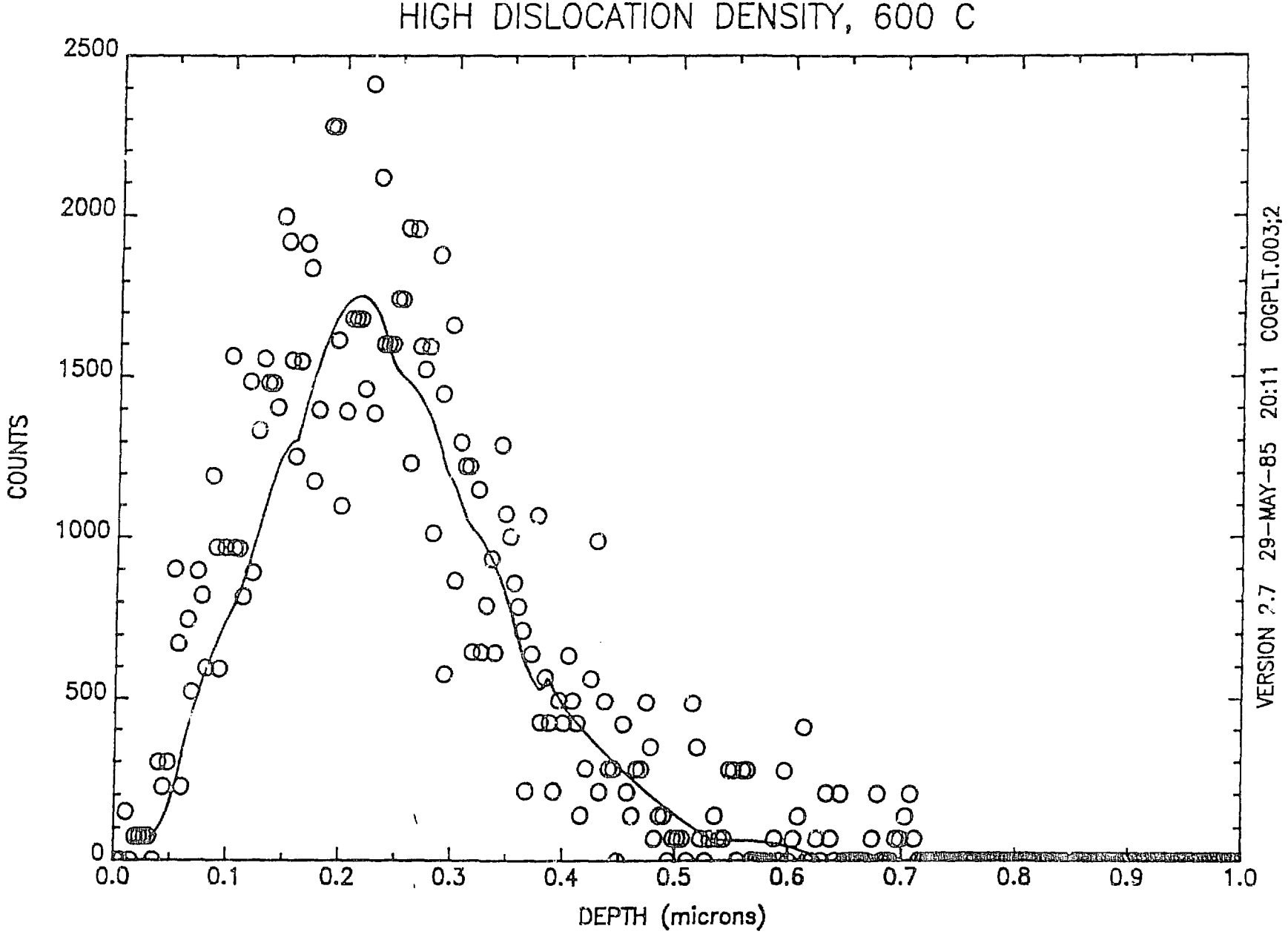
HIGH DISLOCATION DENSITY, 600 C
COUNTS
2500
2000
1500
1000
500
0
0.0
0.1
0.2
0.3
0.4
0.5
0.6
0.7
0.8
0.9
1.0
DEPTH (microns)
VERSION 2.7 29-MAY-85 20:11 COGPLT.003;2

Figure 6

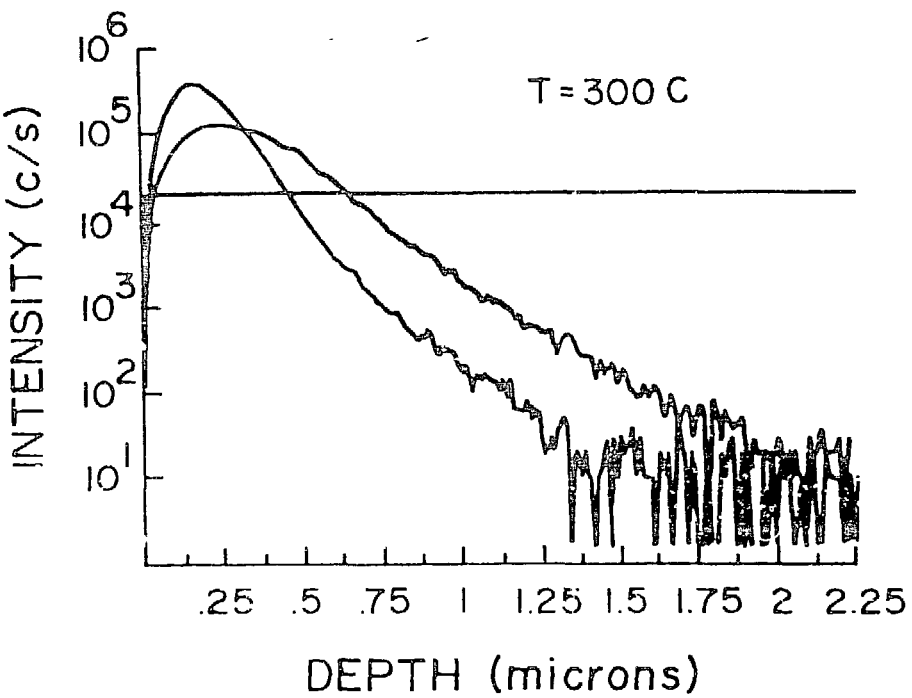
T = 300 C
INTENSITY (c/s)
10^6
10^5
10^4
10^3
10^2
10^1
.25 .5 .75 1 1.25 1.5 1.75 2 2.25
DEPTH (microns)

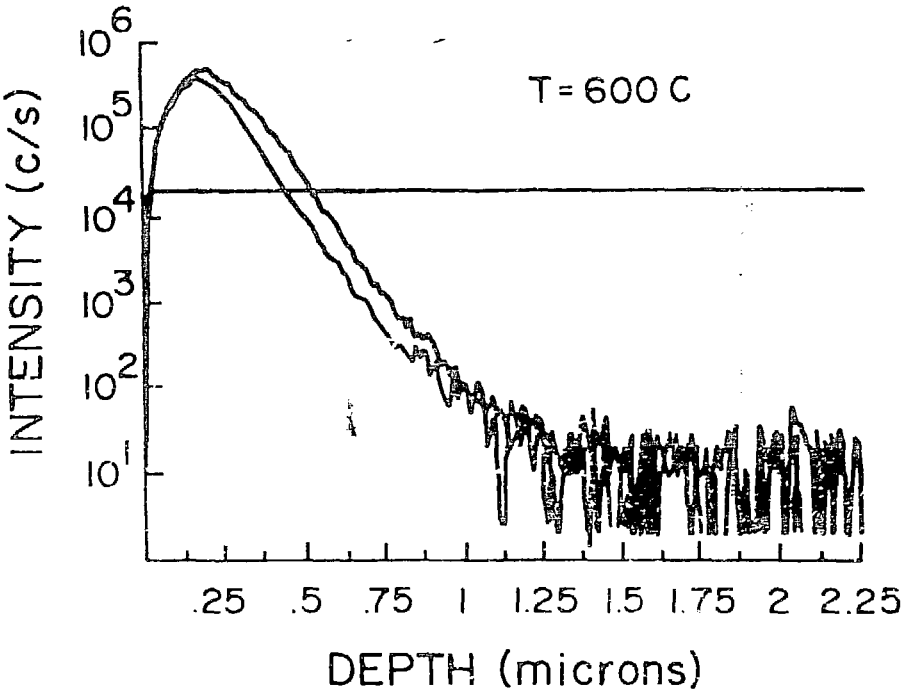
INTENSITY (c/s)
10^6
10^5
10^4
10^3
10^2
10^1
T = 600 C
.25
.5
.75
1
1.25
1.5
1.75
2
2.25
DEPTH (microns)

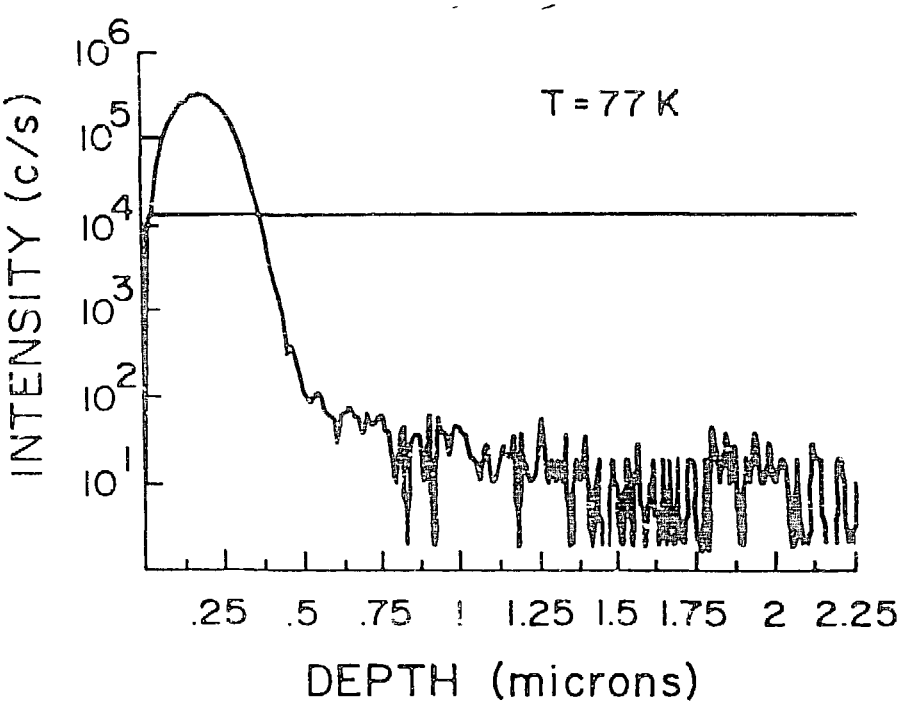
INTENSITY (c/s)
10^6
10^5
10^4
10^3
10^2
10^1
T = 77 K
.25
.5
.75
1
1.25
1.5
1.75
2
2.25
DEPTH (microns)

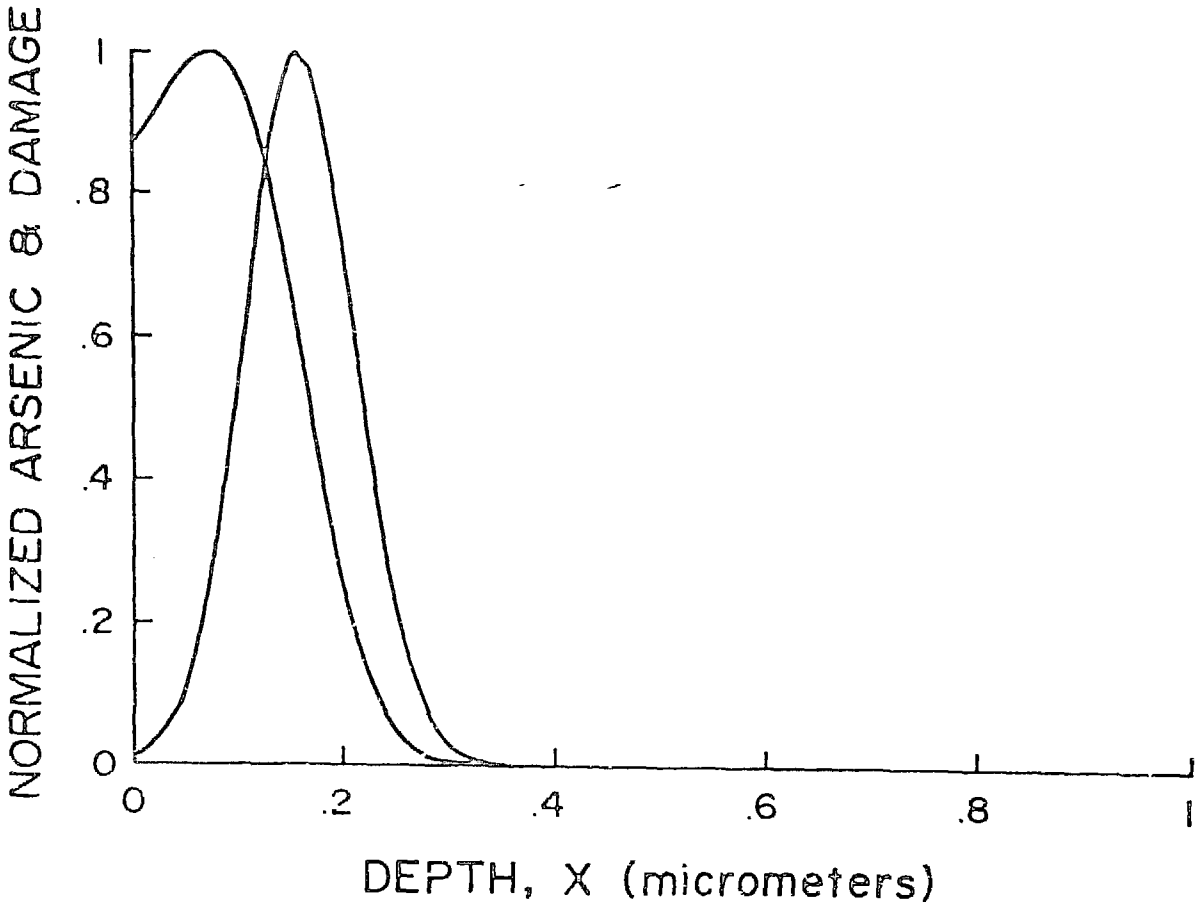

DISCLAIMER

This report was prepared as an account of work sponsored by an agency of the United States Government. Neither the United States Government nor any agency thereof, nor any of their employees, makes any warranty, express or implied, or assumes any legal liability or responsibility for the accuracy, completeness, or usefulness of any information, apparatus, product, or process disclosed, or represents that its use would not infringe privately owned rights. Reference herein to any specific commercial product, process, or service by trade name, trademark, manufacturer, or otherwise does not necessarily constitute or imply its endorsement, recommendation, or favoring by the United States Government or any agency thereof. The views and opinions of authors expressed herein do not necessarily state or reflect those of the United States Government or any agency thereof.